Proton Transfer Dynamics in Acetylacetone: A Mixed Quantum-Classical Simulation of Vibrational Spectra

Janez Mavri* and Jože Grdadolnik

National Institute of Chemistry, Hajdrihova 19, 1000 Ljubljana, Slovenia

Received: October 5, 2000

Proton dynamics in the medium-strong intramolecular hydrogen bond of acetylacetone (Pentane-2,4-dione) was studied using the mixed quantum-classical method density matrix evolution (DME). The proton involved in the hydrogen bond was treated as a quantum particle, involving several vibrational levels, while the rest of the system was treated using classical mechanics. Molecular simulations were performed in the gas phase and in a chloroform solution. The effects of deuteration were also considered. The vibrational spectrum was calculated by Fourier transform of the time-dependent expectation value for the OH bond length. In the present case, we demonstrate by calculations and experimentally that coupling of the proton to the OO and both CO bonds, which are attached to the hydrogen bond (indirect relaxation mechanism) is more important than coupling to the solvent degrees of freedom in determining spectral shape.

1. Introduction

Proton-transfer processes are of central importance for chemistry and biochemistry. Much experimental and theoretical work has been associated with studies of these types of processes. One of the manifestations of proton dynamics in hydrogen bonds involving oxygen atoms as proton donors and proton acceptors is a broadening of the asymmetric OH stretching band found in vibrational spectra.

From the shape of the vibrational spectrum one can draw conclusions about the strength of the hydrogen bond and the shape of the proton potentials. A broad band is characteristic for strong hydrogen bonds OH..O and can be assigned to asymmetric OH stretching. The half-width of this band often exceeds 2000 cm^{-1}. On the other hand, weak hydrogen bonds are associated with a high proton potential barrier, which is typically associated with a high degree of asymmetry and a much less pronounced broadening of the OH band that appears at high frequency. A lot of effort has been directed toward explaining the infrared spectral density of weak hydrogen bonds.[1−4] For a recent review see ref 5. The physical mechanism causing the vibrational band broadening in solution has been a subject of heated debate. For a general discussion concerning the coupling effects on vibrational spectra see ref 6. Two mechanisms have been proposed. In indirect mechanisms, the OH vibration is coupled to the OO vibration and possibly to some other intramolecular low-frequency modes of the hydrogen-bonded system.[7,8] Zundel and co-workers interpreted the broadening of vibrational bands of strong hydrogen bond systems in polar solution to be caused by coupling the OH vibration to the fluctuations of the orientational polarization of the solvent, the so-called direct mechanism.[9,10]

Hydrogen-bonded complexes in polar solution represent complex systems that cannot in general, be treated analytically. However, molecular simulations like molecular dynamics or Monte Carlo can treat such systems numerically. Recently, a number of molecular simulations have addressed the issue of proton transfer.[11−49]

The proton is a light particle with a de Broglie wavelength of 0.3 Å at room temperature. Classical mechanics is generally inadequate for its treatment. Classical molecular dynamics simulations are based on the premise that atomic nuclei obey the laws of motion of classical mechanics on the Born−Oppenheimer (BO) hypersurface.[50] The BO hypersurface and the forces associated therewith are either rigorously calculated at every time instant, as is the case in the Car−Parrinello scheme[51] or approximated by computationally inexpensive empirical atom to atom function. The results of classical MD simulations become questionable when (i) high-frequency vibrations, (ii) optical transitions, or (iii) proton transfer take place. Proper theoretical treatment of such processes requires quantum-dynamical methods. With currently available computer power it is possible to treat only a few degrees of freedom quantum-dynamically. A possible solution to this consists of mixing quantum and classical worlds by embedding the quantum subsystem in a classical environment.

Several methods have been developed for the treatment of mixed quantum-classical systems. Path integral (PI) simulations[20,21] are based on the isomorphism between the quantum particle and a necklace of beads. The difficulty in getting PI methods to yield meaningful time-dependent quantities has recently been overcome by the introduction of the centroid dynamics PI method.[18,19] Recently, the Car−Parrinello method has been combined with the path integral approach.[52,53] Wave packet dynamics is another powerful method for mixed quantum-classical dynamics.[54] Bala et al.[14−17] applied this method to the theoretical treatment of proton transfer in an enzymatic reaction. Moreover, it was shown[16] that the wave packet method yielded results practically identical to those of the density matrix evolutions (DME) method for the transferred energy when a collinear collision between the quantum harmonic oscillator and a classical atom was considered (vide infra). The surface hopping (SH) scheme with the least number of switches[55] mainly differs from the DME scheme in the sense that the force acting from the quantum system corresponds to the pure quantum state.

* To whom correspondence should be addressed. E-mail: janez@kihp2.ki.si.

10.1021/jp003671s CCC: $20.00
Published on Web 02/08/2001

The abrupt switching between the quantum states is associated with a probabilistic algorithm involving a random number generator. To conserve the total energy, ad hoc scalings of the velocities for the classical particles are necessary. The number of switches between the quantum states should be kept low. Any abrupt transitions between the quantum states are justified by semiclassical arguments. It is, however, worth emphasizing that there is no rule in quantum mechanics that would postulate the application of either the pure quantum state or mixed state for calculation of the force.

The DME method[56] is based on the coupling of the Liouville−von Neumann equation (for the quantum subsystem) with the classical equations of motion with which the rest of the system is described. The coupling is performed in a self-consistent way such that the total energy is a constant of motion. The main characteristic of the DME method is that the force acting on the classical subsystem originates from the mixed quantum state and therefore means that DME belongs to the class of methods that use Ehrenfest approach. The DME method has been applied to a variety of systems: treatment of collisions of the quantum harmonic oscillator and noble gas atoms[57−59] and calculation of rate constants for the proton-transfer processes in aqueous solution[34,35] and enzymatic environments.[60]

In this article the dynamics of proton transfer in the intramolecular hydrogen bond of acetylacetone (ACAC) in chloroform solution is addressed. Asymmetric OH stretching in ACAC is treated quantum-dynamically, while all other degrees of freedom are treated by classical mechanics. The effects of deuteration are also studied. The proton is tightly coupled to the OO and both CO bond stretchings. These degrees of freedom significantly distort the proton potential and the proton "feels" them to be almost frozen. In the studied system, intramolecular coupling is more important than coupling with chloroform. The vibrational spectra are calculated from the time-dependent expectation value of OH bond length and are compared with the experimental spectra.

2. Proton Potential in Acetylacetone

The intramolecular proton potential in ACAC was calculated using the density functional theory on the B3LYP/6-311+G-(2d,2p) level and was fitted to a two-state empirical valence bond (EVB) form. For all details of the EVB description of ACAC see ref 61. The currently used EVB form is computationally inexpensive and is therefore suitable for numerical calculations of the several matrix elements used in this study. The proton potential depends on the OO distance and both CO distances. Elongation of the OO distance gives rise to an elevation of the barrier, while CO bond length fluctuations introduce asymmetry to the proton potential. Apart from the CO..H..CO moiety of ACAC, the rest of the intramolecular degrees of freedom are described using the standard GROMOS-87 force field[62] for bond length, bond angles, and proper and improper dihedral angles. All intramolecular nonbonding interactions are excluded. Both methyl groups are treated as united atoms. The interaction energy between ACAC and chloroform is described by 12-6-1 terms. The atomic charges are calculated using the Besler−Merz−Kollman procedure,[63] which fits the charges in such a way that they reproduce the electrostatic potential in the vicinity of the molecule. The fitting was performed with an included solvent reaction field using the method of Miertuš et al.[64] implemented in the Gaussian-94[65] suite of programs. Thus, calculated atomic charges correspond to the effectively polarized values. The atomic charges critically depend on the OH bond length. Atomic charges are determined for the OH bond lengths corresponding to its value for the reactants, transition states, and the products. Only two calculations were required, due to the symmetry of reactants and the products. For the other OH values the atomic charges are calculated by parabolic interpolation. Variations in the atomic charges with respect to the OO and CO distances are not considered in this study. The variation of the atomic charges with the proton transfer can be compared with the approach proposed by Hynes and co-workers.[47,43,49] The applied Lennard-Jones parameters are from the GROMOS-87 force field.[62] Standard combination rules are used for calculating interaction energies and the force for ACAC-solvent and solvent−solvent. The Lennard-Jones part of the potential thus reads $V_{LJ} = 4\epsilon_{ij}((\sigma_{ij}/r_{ij})^{12} - (\sigma_{ij}/r_{ij})^{6})$, where $\sigma_{ij} = (\sigma_i + \sigma_j)/2$ and $\epsilon_{ij} = (\epsilon_i\epsilon_j)^{1/2}$. The nonbonding parameters used in this study are shown in Table 1.

TABLE 1: Nonbonding Parameters Used for the Molecular Dynamics Simulation of acetylacetone in chloroform solution[a]

atom	σ	ϵ	q_R	q_{TS}	q_P
O1	2.870	0.2415	−0.597	−0.624	−0.621
C2	3.361	0.0970	0.679	0.745	0.784
C3	3.361	0.0970	−0.855	−−0.902	−0.855
C4	3.361	0.0970	0.784	0.745	0.679
O5	2.870	0.2415	−0.621	−0.624	−0.597
C6	3.786	0.1800	−0.003	−0.039	−0.070
C7	3.786	0.1800	−0.070	−0.039	−0.030
H8	0.044	0.046	0.239	0.250	0.239
H9	0.0	0.0	0.471	0.488	0.471
$C^{(s)}$	3.400	0.1017	0.179		
$H^{(s)}$	2.202	0.0197	0.082		
$CL^{(s)}$	3.440	0.2995	−0.087		
$CL^{(s)}$	3.440	0.2995	−0.087		
$CL^{(s)}$	3.440	0.2995	−0.087		

[a] The atomic labels for acetylacetone correspond to those in Figure 1. The atoms assigned with a superscript (s) correspond to chloroform. The charges q_R, q_{TS}, and q_P correspond to the Merz−Kollman atomic charges for the reactants, transition states, and the products of the proton transfer in acetylacetone.

3. Flexible Chloroform Model

We applied the chloroform model proposed by Tironi and van Gunsteren.[66] This is an all-atom model and nicely reproduces experimental density and heat of evaporation. The original chloroform model is rigid and, therefore, requires the application of holonomic contraints such as SHAKE[67] in molecular dynamics simulations. We introduced the flexible chloroform model here in order to have nuclear polarization and dynamic coupling between the chloroform's intramolecular degrees of freedom and ACAC vibrations. Since we wanted to keep a simple GROMOS functional form for the solvent, we modeled the molecule using harmonic bond lengths and harmonic bond angles with no cross terms. The force constants were adjusted such that the calculated vibrational frequencies in the harmonic approximation fit the experimental values. We gave special attenton to low frequencies, which contribute significantly to the thermodynamics, and to high frequencies (above 2000 cm^{-1}), which might be coupled to the OH vibrations. The harmonic force constant for C−H stretching is 361.8 kcal mol^{-1} $Å^{-2}$, while for C−Cl strething it is 180.9 kcal mol^{-1} $Å^{-2}$. The harmonic force constant for Cl−C−H bending is 41.6 kcal mol^{-1} rad^{-2}, while for Cl−C−Cl bending it is 93.7 kcal mol^{-1} rad^{-2}. The experimental and calculated frequencies in the harmonic approximation are shown in Table 2. Agreement of the calculated frequencies with the experimental values is fairly

TABLE 2: Calculated and Experimental Vibrational Frequencies (cm^{-1}) of the Applied Chloroform Model[a]

description	calculated	experimental
symm CH stretching	3033	3033
symm C−Cl_3 stretching	589	674.5
Cl−C−Cl bending	288	364
H−C−Cl bending	1219	1219
antisymm C−Cl_3 stretching	796	772
antisymm C−Cl_3 bending	261.8	262

[a] Assignation of the frequencies was performed by visualization of the normal modes.

good. Determination of the dielectric constant using molecular simulation is based on the distribution of the dipole moment and it requires extremely long runs. The dielectric constant was not calculated either for the original, rigid, chloroform or for the present, flexible, model. Although it is believed that the major contribution to the dielectric constant originates from the orientational polarization, it would be a challenge to study the effect of the flexibility on the dielectric constant.

4. Simulation Methods

The density matrix evolution (DME) method, which allows the simulation of a quantum-dynamical subsystem embedded in a classical environment, was applied for the simulation of intramolecular proton tranfer in ACAC. The DME method is based on coupling of the Liouville−von Neumann equation (for the classical subsystem) with the classical equations of motion (for the rest of the

system). The coupling is self-consistent; i.e., the total energy and the total momentum are both constants of motion.

In the DME method the wave function of the quantum subsystem was expanded on a properly chosen orthonormal time-independent basis set ϕ.

$$\Psi(\xi,t) = \sum_{n=1}^{M} c_n(t)\,\phi_n(\xi) \tag{1}$$

where ξ denotes the coordinate(s) of the quantum subsystem. The time propagation of the quantum subsystem was performed using time dependence of the coefficients in a linear combination. The $M \times M$ density matrix $\boldsymbol{\rho}$ is defined as $\rho_{nm} = c_n c_m^+$, where M is the number of basis functions applied in a linear combination. Diagonal elements represent the populations of the levels, while off-diagonal elements contain phase (coherence) information.

The $\mathbf{H}^0$ matrix elements were calculated numerically, where $H^0_{nm} = \langle n|H^0|m\rangle$ and H^0 stand for the Hamiltonian of the unperturbed quantum system. The perturbation Hamiltonian matrix elements can be calculated from

$$H'_{nm}(\mathbf{R}) = \langle n|H'(\mathbf{R})|m\rangle \tag{2}$$

where $\mathbf{R}$ are the coordinate(s) of the classical particle(s) and $H'(\mathbf{R})$ stands for the interaction between the quantum and the classical subsystems. The Hamiltonian matrix $\mathbf{H}(\mathbf{R})$ is calculated by summing $\mathbf{H}^0$ and $\mathbf{H}'(\mathbf{R})$, and the energy of the quantum subsystem is calculated as

$$E_{\mathrm{Q}} = \mathrm{Tr}(\boldsymbol{\rho}\mathbf{H}(\mathbf{R})) \tag{3}$$

This energy includes the kinetic energy of the quantum subsystem, as well as the total potential energy of the combined system; the kinetic energy of the classical system and the interaction energy between the classical particles are not included.

TABLE 3: Basis Applied in the DME Calculation[a]

x_0	α
1.045	22.6
1.145	18.2
1.245	17.4
1.345	18.2
1.445	22.6

[a] The basis functions are simple, one−dimensional Gaussians that read $\Phi_i = N_i \exp(-\alpha(\xi - x_0))$, N_i are normalization factors, x_0 (Å) are the Gaussian centers given as the distances from the proton donor, and α ($Å^{-2}$) are the exponents. Centers of the Gaussians are confined to the OO line.

In DME the coupling between the classical degrees of freedom within the quantum subsystem proceeds via the concept of the Hellmann−Feynman force matrix. The force, $F^Q_{\mathbf{R}}$, exerted by the quantum subsystem on any classical particle coordinate $\mathbf{R}$ is the expectation value of $-\partial H/\partial \mathbf{R}$, such that

$$F^Q_{\mathbf{R}} = \mathrm{Tr}(\boldsymbol{\rho}\mathbf{F}_{\mathbf{R}}) \tag{4}$$

The Hellmann−Feynman force matrix elements are defined as

$$F_{\mathrm{nm},\mathbf{R}} = \left\langle n\left| -\frac{\partial \mathrm{H}}{\partial \mathbf{R}}\right| m\right\rangle \tag{5}$$

The density matrix evolves with time according to the Liouville-von Neumann equation

$$\dot{\rho} = \frac{i}{h}(\boldsymbol{\rho}\mathbf{H} - \mathbf{H}\boldsymbol{\rho}) \tag{6}$$

The classical equations of motion are integrated with a velocity form of the Verlet algorithm using a time step of 1.0 fs. This is an accurate integrator that requires two evaluations of the force per time step. The Liouville−von Neumann equation is integrated as a set of the ordinary differential equations of the first order using the Runge−Kutta integrator of the fourth order with a time step of 0.02 fs. When integrating classical atoms one step forward the wave function representing the proton is kept frozen; however when propagating the wave function forward, the classical degrees of freedom are fixed. The proton was modeled as a one-dimensional quantum particle using five displaced simple Gaussians as basis functions. Simple Gaussians are zero-order Gauss-Hermite polynomials that are eigenfunctions of the quantum harmonic oscillator. Displaced simple Gaussians are therefore suitable basis functions for describing vibrational states. The basis functions are placed on a line connecting the proton donor and the proton acceptor. During dynamics the basis set is attached to the bisector of the OO bond and moves with it. The proton potential corresponding to the ACAC structure with equal CO distances of 1.284 Å, and an OO distance of 2.523 Å was chosen as the reference state for the calculation of $\mathbf{H}^0$. The equilibrium positions and the exponents of the Gaussians are optimized so that the variationally calculated eigenvalues match the exact eigenvalues for a given potential, calculated numerically by the shooting method. The parameters of the applied basis set are shown in Table 3. The basis set is orthogonalized using the canonical method.[68] All the matrix elements apart from the overlap and the kinetic energy are calculated numerically using an accurate 30 point Gauss−Legendre quadrature. The matrix elements are calculated

over the original basis set. The matrix elements are calculated over the orthogonal basis set[35] using the transformation given elsewhere.

For simulations of ACAC in chloroform solution the solute is embedded in a cubic box of chloroform with an edge of 22 Å The spherical cutoff treatment using the shifted force method[69] was employed. The cutoff radii of 10 and 8 Å for the long- and short-range spherical cutoffs were used. The authors have demonstrated improved results for simulations performed using the shifted force scheme compared with the results of the simulation using the applied conventional potential cutoff.[69] The classical atoms are coupled to the thermal bath using a Berendsen's thermostat[70] with a reference temperature of 298 K and with a coupling constant of 0.1 ps. The condensed phase simulations are performed at a constant volume. In the simulation with no coupling to the thermal bath the drift of the total energy is negligible. This confirms that the applied time steps are small enough and that long-range electrostatics is treated properly. After a careful equilibration of 50 ps, the simulation runs are continued for 200 ps. The trajectory, including the density matrix is stored every 4 fs in order to have sufficient resolution to calculate the vibrational spectra. Vibrational spectra are calculated from the time-dependent expectation value of the proton position using the fast Fourier transform technique. Electrical harmonicity of the hydrogen bond was assumed; i.e., the change of the dipole moment was assumed to be proportional to the elongation of the OH bond. In principle, a spectrum calculated in this way contains all the vibrational modes associated with the simulated system. In the present study, only the OH stretching is treated quantum-dynamically, while all other degrees of freedom are treated classically. Such treatment does not allow for a quantitative comparison between the experimental and calculated parts of the spectra for bands not associated with asymmetric OH stretching. A Gaussian filter is applied in order to correct for the artifacts associated with the finite length samples.

5. Vibrational Spectra

We performed measurements of the infrared spectra of acetylacetone in 0.1 M chloroform solution, of deuterated acetylacetone in chloroform solution, and of acetylacetone in the gas phase. An infrared spectrometer Perkin-Elmer system 2000 was used for all the measurements. A gas cell with the optical length of 10 m was used for gas phase measurements. Although all experiments, apart from the gas phase, had been performed previously,[71,72] we decided to repeat the IR measurements. The solvent contribution was subtracted for spectra recorded in solution. The spectra measured by us are in perfect agreement with the previous measurements.

The experimental vibrational spectrum of acetylacetone in chloroform solution shows a broad asymmetric OH stretching band between 1800 and 3400 cm^{-1} with a center at 2750 cm^{-1} (Figure 2). The strong peak at about 1550 cm^{-1} corresponds to carbonyl stretchings. The peak at roughly 2300 cm^{-1} was assigned to the traces of carbon dioxide, while peaks slightly above 3000 cm^{-1} could be assigned to the ACAC methyl group vibrations. A narrow peak at 1600 cm^{-1} was assigned to the keto form of ACAC.

The spectrum of deuterated ACAC in $CDCl_3$ is shown in Figure 3. Upon deuteration the band associated with asymmetric OD stretching shifts down to 1950 cm^{-1}, consistent with the earlier assignment.[71,72] The OD peak spreads between about 1800 and 2500 cm^{-1}, although the boundary where the peak ends is somewhat arbitrary, due to the fact that the peak is broad and weak. The peak appearing roughly at 3000 cm^{-1} could, again, be assigned to the methyl group vibrations and the unexchanged H.

Broad absorption bands are characteristic for the strong hydrogen bonds. The bands are red shifted upon deuteration. These features are observed in the measured spectra shown in Figures 2−4. The ring associated with the intramolecular hydrogen bond in ACAC is a conjugated system associated with a high electronic polarizability and a low intensity of the OH asymmetric stretching.

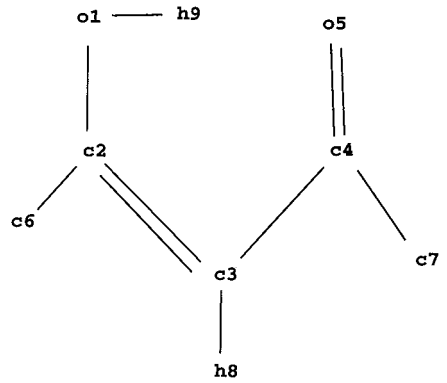

Figure 1. Structure of the enol tautomer of acetylacetone.

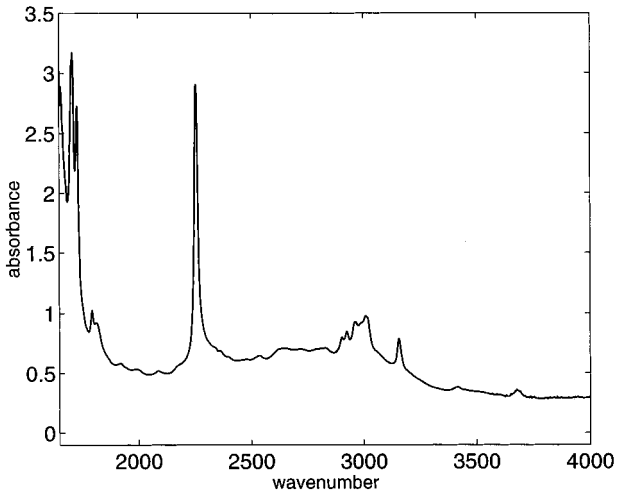

Figure 2. Experimental IR spectrum of acetylacetone in 0.1 M $CHCl_3$ solution.

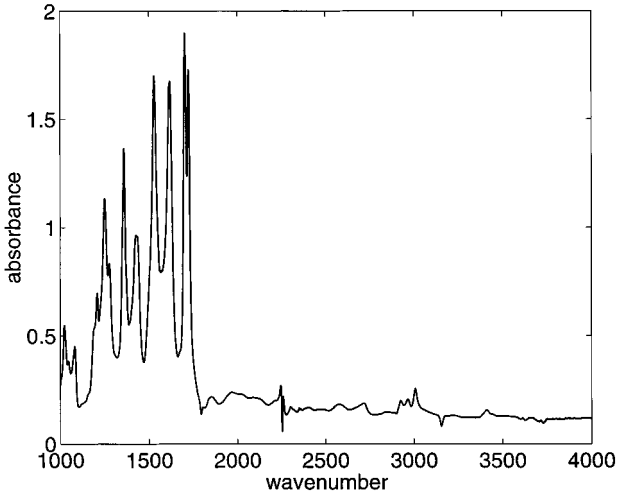

Figure 3. Experimental IR spectrum of deuterated acetylacetone in 0.1 M $CDCl_3$ solution.

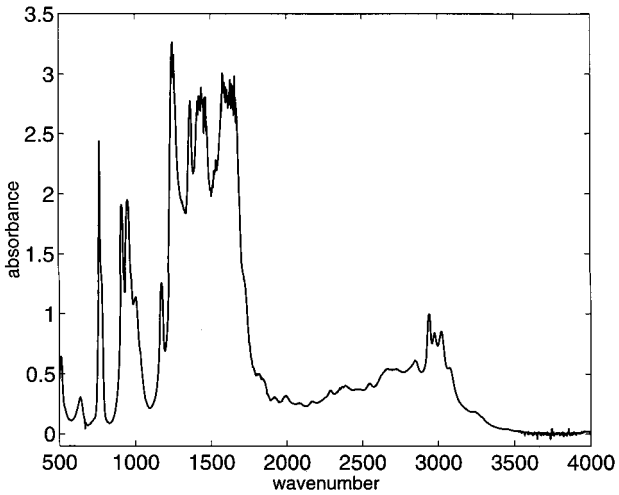

Figure 4. Experimental IR spectrum of acetylacetone in the gas phase.

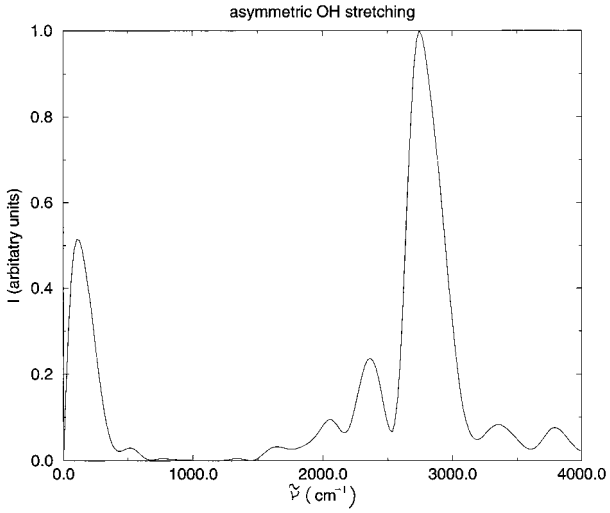

Figure 5. Simulated spectrum of acetylacetone in chloroform solution.

The gas phase spectrum is shown in Figure 4. The band position and the shape corresponding to the asymmetric OH stretching after subtracting the chloroform signal are not significantly different from those found in the gas-phase spectra. The assignation is the same as for ACAC in chloroform solution, except that the signal associated with the keto form is absent. Therefore, there is strong experimental evidence for the dominant role of the indirect coupling mechanism in the broadening of the vibrational spectrum in acetylacetone.

The quantum-dynamically calculated vibrational spectra are shown in Figures5−7. The asymmetric OH stretching band center appears at about 2800 cm^{-1}, and it spreads between 2000 and 3700 cm^{-1}. The corresponding simulated band in the gas phase (Figure 6) is very similar to that found in chloroform solution, although it is somewhat narrower. We cannot simply explain the fine structure of the OH stretching band (Figure 5). The mixed quantum-classical simulation used in the present work is a numerical experiment with all the advantages and disadvantages inherent to such treatment.

Upon deuteration the simulated OD stretching peak drops to 2000 cm^{-1} (Figure 7). The peak remains broad and spreads between 1600 and 2700 cm^{-1}. The simulated peak (Figure 5) with the center at about 250 cm^{-1} can be assigned to the OO stretching, while the weak peak occurring at about 1600 cm^{-1} can be explained by carbonyl stretchings. Such description of the OO stretching deserves some comment. We are aware that several normal vibrational modes contribute to the variation in

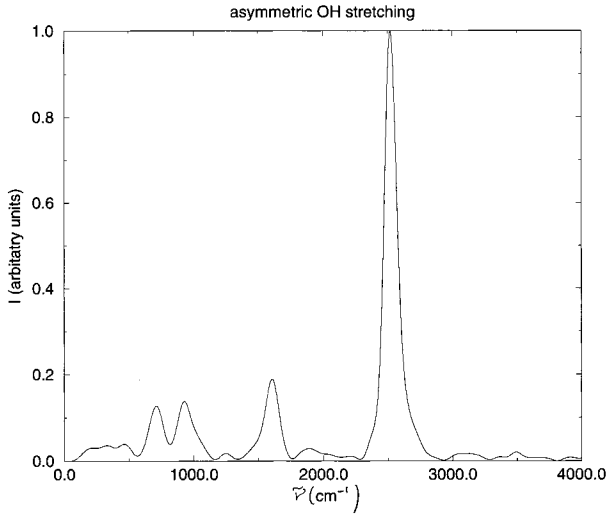

Figure 6. Simulated spectrum of acetylacetone in the gas phase.

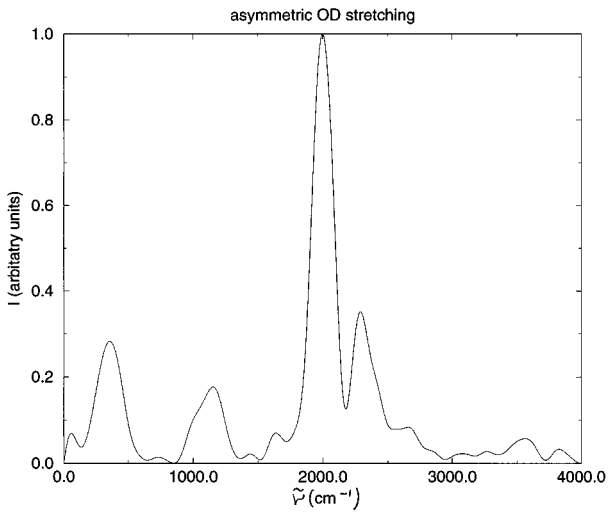

Figure 7. Simulated spectrum of deuterated acetylacetone in chloroform solution.

the OO distance. In principle one should couple each of them explicitly to the proton potential. Since the parametrization of such coupling would be computationally too expensive, we decided to treat the OO distance as a special mode, following the approach of Borgis and Hynes.[73] Visualization of the molecular dynamics trajectory confirms the assignment. Moreover, we performed the Fourier transform of the OO distance as a function of time and once more confirmed the assignment. In the present study, the change of the dipole moment associated with the other intramolecular degrees of freedom, except the OH stretching, was not quantitatively taken into account. Of the intramolecular degrees of freedom, only the OO and the two CO were coupled to the asymmetric OH stretching. Therefore, the relative intensities of the other peaks are not directly comparable to the experimentally derived values. Moreover, the present simulations are relatively short (50 ps equilibration followed by 200 ps sampling) and it is possible that the equilibration is not perfect, specially for the gas-phase simulation.

In one simulation, the intramolecular degrees of freedom of ACAC in chloroform solution were frozen. The OO distance was 2.543 Å and both CO distances were 1.284 Å. This resulted in a symmetric double-well potential for the gas phase. The calculated asymmetric OH stretching of rigid ACAC in chloroform solution resulted in a narrow band with a center at about

1100 cm^{-1} and a half-width of about 100 cm^{-1} (not shown), which does not reproduce the experimental situation. This is additional proof of the importance of intramolecular (indirect) coupling for the shape of the band asociated with asymmetric OH stretching in ACAC.

6. Conclusions and Perspectives

Calculations of vibrational spectra of acetylacetone (ACAC) in chloroform solution and in the gas phase were performed with molecular dynamics simulations using density matrix evolution, a mixed quantum dynamical-classical method. The present study demonstrates that it is possible to simulate the vibrational spectrum of strong hydrogen-bonded systems in polar solution. The simulated bands corresponding to asymmetric OH (OD) stretching match the experimental positions and, in part, their shapes. We demonstrate the importance of intramolecular coupling in acetylacetone for the shape of the OH band. It is worth emphasizing that the vibrational spectrum is extremely sensitive to all details of the simulation, especially to the applied force field, since it involves second derivatives of the potential. Therefore, calculation of the vibrational spectra of hydrogen-bonded systems offers a possibility for fine-tuning of the force fields. During quantum-dynamical treatment, the Born−Oppenheimer hypersurface is sampled around the levels of the ground and the first vibrational states, not only around the classical minimum. The primary aim of the present work is calculation of the OH stretching band. The OH stretching was treated quantum-dynamically, and the information concerning the dipole moment was properly included. The information concerning the change of the dipole moments associated with the other modes, including the solvent, was not directly taken into account. The appearance of the other modes is therefore reflected in the calculated spectrum only via their couplings to the OH stretching. Our approach is closely related to the simulation of Zundel polarization in a model strong hydrogen-bonded system.[13] Our approach is related to the experimental situation where the solvent signal is subtracted.

To reproduce the vibrational spectrum of the present system (i.e., the band associated with asymmetric OH or OD stretching), it was necessary to examine the proton potential on a high, computationally intensive (B3LYP/6-311+G(2d,2p)) level and fit it to a computationally tractable empirical valence bond form. The spectrum was calculated from first principles using a mixed quantum-classical MD. Chloroform was treated in atomic detail and no "bath" approximation for the solvent was necessary. Since the solvent's electronic degrees of freedom follow the proton, one needs, in principle, a polarizable solvent model. Applications of the polarizable solvent model will be preferred for future simulations of the proton transfer processes. Since the simulated spectrum is very sensitive with respect to the applied force field and other parameters of the simulation, it can be used for fine-tuning the simulation parameters. In the present study, the OO and CO vibrations were treated by classical mechanics. However, quantum-dynamical treatment of these degrees of freedom would be highly desirable and we hope to apply it in future studies.

The DME method has many possible applications. Simulation of proton transfer in the Mannich bases in polar solution[74] is also a possible future application of the DME method. Inclusion of the external electromagnetic field into the mixed quantum-classical simulation is possible[44−46] and offers a possibility for computational support of the pulse-echo experiments in the infrared region. We hope to apply this method in the near future. Replacement of the polar solvent with a fluctuating macromolecular environment, such as an enzyme, is methodologically a straightforward step but requires a lot of coding effort. We hope to apply the DME method for the treatment of enzymatic reactions in the near future.

Finally, we would like to say a few words about the validity of the DME method. Full quantum treatment is currently possible for only four atoms. Mixing of the quantum and classical degrees of freedom always involves an approximation. The basic difference between surface hopping (SH) and DME is that, in the former case, the force acting on the classical subsystem originates from the pure quantum states, while, in the latter case, the force corresponds to its expectation value. Neither DME nor SH can be derived from the Schrödinger equation. For certain applications one method gives better results, while for some other applications the other method proves better. For the proton-transfer processes we have shown that both methods give comparable results,[75] which can be contrasted with the results of Fang et al.[42] There is still room for further development of the methods involved in mixed quantum-classical dynamics and its application for proton-transfer processes in complex environments.

Acknowledgment. We are grateful to Prof. Dušan Hadži and Prof. Jure Zupan, National Institute of Chemistry, Slovenia, and Prof. Benoit Roux, University of Montreal, for many stimulating discussions and a critical reading of the manuscript. We thank Dr. Ilario Tironi, ETH Zürich, for providing us with the coordinates of the equilibrated chloroform simulation box and to Dr. Milan Hodošček, National Institute of Chemistry, Slovenia, for his assistance with the flexible chloroform model. We are also grateful to Ms. Charlotte Taft for linguistic corrections and the referee for many useful comments. This work was supported by a grant from the Slovenian Ministry of Science and Technology.

References and Notes

(1) Borstnik, B. *Chem. Phys*. **1976**, *15*, 391.
(2) Hadži, D.; Bratos, S. In *The Hydrogen Bond Theory*; Schuster, P., Zundel, G., Sandorfy, C., Eds.; North-Holland: Amsterdam, 1976; p 567.
(3) Marechal, Y. *J. Chem. Phys*. **1987**, *87*, 6344.
(4) Witkowski, A.; Wojcik, M. *Chem. Phys*. **1973**, *1*, 9.
(5) Henri-Rousseau, O.; Blaise, P. In *Advances in Chemical Physics*; Prigogine, I., Rice, S. A., Eds.; J. Wiley: New York, 1998; Vol. 103, pp 1−186.
(6) Wood, K. A.; Strauss, H. L. *J. Phys. Chem*. **1990**, *94*, 5677−5684.
(7) Bratos, S. *J. Chem. Phys*. **1975**, *63*, 3499.
(8) Bratos, S.; Ratajczak, H. *J. Chem. Phys*. **1982**, *67*, 77.
(9) Janoschek, R.; Weideman, E. G.; Pfeifer, H.; Zundel, G. *J. Am. Chem. Soc*. **1972**, *94*, 2387.
(10) Zundel, G. *Proton Polarizability of Hydrogen Bonds and Proton-Transfer Processes, Their Role in Electrochemistry and Biology*; Institut für Physikalische Chemie der Universität München: Germany, 1997.
(11) Laria, D.; Ciccotti, G.; Ferrario, M.; Kapral, R. *J. Chem. Phys*. **1992**, *97*, 378−388.
(12) Borgis, D.; Tarjus, G.; Azzouz, H. *J. Phys. Chem*. **1992**, *96*, 3188−3191.
(13) Borgis, D.; Tarjus, G.; Azzouz, H. *J. Chem. Phys*. **1992**, *97*, 1390−1400.
(14) Bala, P.; Lesyng, B.; Truong, T. N.; McCammon, J. A. In *Molecular Aspects of Biotechnology: Computational Models and Theories*; Bertran, J., Ed.; Kluwer: Dordrecht, The Netherlands, 1992; pp 299−326.
(15) Bala, P.; Lesyng, B.; McCammon, J. A. *Chem. Phys*. **1994**, *180*, 271−285.
(16) Bala, P.; Lesyng, B.; Truong, T. N.; McCammon, J. A. In *Quantum Mechanical Simulation Methods for Studying Biological Systems*; Bicout, D., Field, M. Eds.; Springer: Berlin, 1996.
(17) Bala, P.; Grochowski, P.; Lesyng, B.; McCammon, J. A. *J. Phys. Chem*. **1996**, *100*, 2535−2545.
(18) Lobaugh, J.; Voth, G. A. *J. Chem. Phys*. **1994**, *100*, 3039−3047.
(19) Lobaugh, J.; Voth, G. A. *J. Chem. Phys*. **1996**, *104*, 2056−2069.
(20) Gillan, M. J. *Philos. Mag. A* **1988**, *58*, 257−283.
(21) Li, D.; Voth, G. A. *J. Phys. Chem*. **1991**, *95*, 10425−10431.

(22) Consta, S.; Kapral, R. *J. Chem. Phys*. **1996**, *104*, 4581−4590.
(23) Hammes-Schiffer, S.; Tully, J. C. *J. Chem. Phys.* **1994**, *101*, 4657−4667.
(24) Hammes-Schiffer, S.; Tully, J. C. *J. Phys. Chem*. **1995**, *99*, 5793−5797.
(25) Hammes-Schiffer, S. *J. Chem. Phys*. **1996**, *105*, 2236−2246.
(26) Drukker, K.; Hammes-Schiffer, S. *J. Chem. Phys*. **1997**, *107*, 363−374.
(27) Fang, J.-Y.; Hammes-Schiffer, S. *J. Chem. Phys.* **1997**, *106*, 8442−8454.
(28) Fang, J.-Y.; Hammes-Schiffer, S. *J. Chem. Phys.* **1997**, *107*, 5727−5739.
(29) Fang, J.-Y.; Hammes-Schiffer, S. *J. Chem. Phys.* **1997**, *107*, 8933−8939.
(30) Morelli, J.; Hammes-Schiffer, S. *Chem. Phys. Lett*. **1997**, *269*, 161−170.
(31) Marx, D.; Parrinello, M. *J. Chem. Phys*. **1996**, *104*, 4077.
(32) Stich, I.; Marx, D.; Parrinello, M.; Terakura, K. *J. Chem. Phys*. **1997**, *107*, 9482−9492.
(33) Tuckerman, M.; Laasonen, K.; Sprik, M.; Parrinello, M. *J. Chem. Phys*. **1995**, *103*, 150−161.
(34) Mavri, J.; Berendsen, H. J. C.; van Gunsteren, W. *J. Phys. Chem*. **1993**, *97*, 13469−13476.
(35) Mavri, J.; Berendsen, H. J. C. *J. Phys. Chem*. **1995**, *99*, 12711−12717.
(36) van der Spoel, D.; Berendsen, H. J. C. Determination of proton-transfer rate constants using ab initio, molecular dynamics, and density matrix evolution calculations. In *Pacific Symposium on Biocomputing 1996*; World Scientific: Singapore, 1995; pp 1−14.
(37) Karmacharya, R.; Schwartz, S. D. *J. Chem. Phys*. **1999**, *110*, 7376−7381.
(38) Cukier, R. I. *J. Phys. Chem. A* **1999**, *103*, 5989−5995.
(39) Loerting, T.; Liedl, K. R. *J. Am Chem. Soc*. **1998**, *120*, 12595−12600.
(40) Vuilleumier, R.; Borgis, D. *Chem. Phys. Lett*. **1998**, *284*, 71−77.
(41) Decornez, H.; Drukker, K.; Hammes-Schiffer, S. *J. Phys Chem. A* **1999**, *103*, 2891−2898.
(42) Fang, J. Y.; Hammes-Schiffer, S. *J. Chem. Phys*. **1999**, *110*, 11166−11175.
(43) Ando, K.; Hynes, J. T. *J. Phys Chem. A* **1999**, *103*, 10398−10408.
(44) Doslic, N.; Kuhn, O.; Manz, J. *Ber. Bunsen-Ges. Phys. Chem*. **1998**, *102*, 292−297.
(45) Doslic, N.; Kuhn, O.; Manz, J.; Sunderman, K. *J. Phys. Chem. A* **1998**, *102*, 9645−9650.
(46) Doslic, N.; Sunderman, K.; Gonzalez, L.; Mo, O.; Kuhn, O. *Phys. Chem. Chem. Phys.* **1999**, *1*, 1249−1257.
(47) Ando, K.; Hynes, J. T. *J. Phys Chem. B* **1997**, *101*, 10464−10478.
(48) Billeter, S.; van Gunsteren, W. *J. Phys. Chem. A* **2000**, *104*, 3276−3286.
(49) Thomson, W. H.; Hynes, J. T. *J. Am. Chem. Soc*. **2000**, *122*, 6278−6286.
(50) van Gunsteren, W. F.; Berendsen, H. J. C. *Angew. Chem., Int. Ed. Engl*. **1990**, *29*, 992−1023.
(51) Car, R.; Parrinello, M. *Phys. Rev. Lett*. **1985**, *55*, 2471−2474.
(52) Marx, D.; Parrinello, M. *Science* **1996**, *271*, 179.
(53) Marx, D.; Hutter, J. *Chapter Ab initio molecular dynamics: Theory and implementations*; John von Neumann Institute for Computing, Forschungszentrum Jülich: Jülich, Germany, 2000; pp 1−149.
(54) Heller, E. J. *J. Chem. Phys*. **1976**, *64*, 63−73.
(55) Tully, J. C. *J. Chem. Phys*. **1990**, *93*, 1061−1071.
(56) Berendsen, H. J. C.; Mavri, J. *J. Phys. Chem*. **1993**, *97*, 13464−13468.
(57) Mavri, J.; Berendsen, H. J. C. *Phys. Rev. E* **1994**, *50*, 198−204.
(58) Mavri, J.; Lensink, M.; Berendsen, H. J. C. *Mol. Phys*. **1994**, *82*, 1249−1257.
(59) Lensink, M. F.; Mavri, J.; Berendsen, H. J. C. *J. Comput. Chem*. **1994**, *17*, 1287−1295.
(60) Mavri, J.; van der Spoel, D.; Berendsen, H. J. C. *J. Phys. Chem*., to be submitted.
(61) Mavri, J.; Grdadolnik, J. *J. Phys. Chem. A* **2001**, *105*, 2039.
(62) van Gunsteren, W. F.; Berendsen, H. J. C. In *GROMOS-87 manual*; Biomos, B.V. Ed.; Nijenborgh 4, 9747 AG Groningen, The Netherlands, 1987.
(63) Besler, B. H.; Merz, K. M., Jr.; Kollman, P. A. *J. Comput. Chem*. **1990**, *11* (4), 431−439.
(64) Miertŭs, S.; Scrocco, E.; Tomasi, J. *Chem. Phys*. **1981**, *55*, 117.
(65) Frisch, M. J.; Trucks, G. W.; Schlegel, H. B.; Gill, P. M. W.; Johnson, B. G.; Robb, M. A.; Cheeseman, J. R.; Keith, T.; Petersson, G. A.; Montgomery, J. A.; Raghavachari, K.; Al-Laham, M. A.; Zakrzewski, V. G.; Ortiz, J. V.; Foresman, J. B.; Cioslowski, J.; Stefanov, B. B.; Nanayakkara, A.; Challacombe, M.; Peng, C. Y.; Ayala, P. Y.; Chen, W.; Wong, M. W.; Andres, J. L.; Replogle, E. S.; Gomperts, R.; Martin, R. L.; Fox, D. J.; Binkley, J. S.; Defrees, D. J.; Baker, J.; Stewart, J. P.; Head-Gordon, M.; Gonzalez, C.; Pople, J. A. *Gaussian 94*, revision B.3; Gaussian, Inc.: Pittsburgh, PA, 1995.
(66) Tironi, I. G.; van Gunsteren, W. F. *Mol. Phys*. **1994**, *83*, 381−403.
(67) Ryckaert, J. P.; Ciccotti, G.; Berendsen, H. J. C. *J. Comput. Phys*. **1997**, *23*, 327−341.
(68) Szabo, A.; Ostlund, N. S. *Modern Qunatum Chemistry*; Macmillan: New York, 1982.
(69) Steinbach, P. J.; Brooks, B. R. *J. Comput. Chem*. **1994**.
(70) Berendsen, H. J. C.; Postma, J. P. M.; DiNola, A.; Haak, J. R. *J. Chem. Phys*. **1984**, *81*, 8.
(71) Bratož, S.; Hadži, D.; Rossmy, G. *Trans. Faraday Soc*. **1956**, *52*, 1956.
(72) Ernstbrunner, E. E. *J. Chem. Soc. A* **1970**, p 1558.
(73) Borgis, D.; Hynes, J. T. *J. Chem. Phys*. **1991**, *94*, 3619−3628.
(74) Fedorowitz, A.; Mavri, J.; Bala, P.; Koll, A. *Chem. Phys. Lett*. **1998**, *289*, 457−462.
(75) Mavri, J. *Mol. Simul*. **2000**, *23*, 389−411.